DEVELOPMENT AND CHARACTERIZATION OF ELECTROSPUN NANOFIBER MEMBRANES FROM POLYAMIDE-6/CELLULOSE ACETATE POLYMERS FOR FILTRATION APPLICATIONS

MUSTAFA YAZICI,[*] İSMAIL TİYEK,[*] MEHMET BARAN KALIN,[**] ÖMER ÖNAL[***] and NESRIN KORKMAZ[****]

[*]*Kahramanmaraş Sütçü İmam University, Kahramanmaraş, Türkiye*
[**]*Osmaniye Korkut Ata University, Osmaniye Vocational School, Osmaniye, Türkiye*
[***]*Tokat Gaziosmanpaşa University, Tokat Vocational School of Higher Education, Tokat, Türkiye*
[****]*Yozgat Bozok University, Hemp Research Institute, Yozgat, Türkiye*
✉ *Corresponding author: M. Yazici, yazici@ksu.edu.tr*

Received May 15, 2026

The increasing demand for high-performance water purification systems has intensified research into advanced filtration materials. In this study, composite nanofiber membranes based on Polyamide-6 (PA6) and cellulose acetate (CA) were fabricated to combine the mechanical strength of PA6 with the hydrophilic and biodegradable characteristics of CA. PA6/CA blend solutions were prepared at weight ratios of 100/0, 75/25, 50/50, 25/75, and 0/100. The morphological and structural characterizations of the electrospun membranes were performed using Scanning Electron Microscopy (SEM) and Fourier Transform Infrared Spectroscopy (FTIR). SEM analyses showed that the addition of CA increased the average nanofiber diameter and promoted the formation of more-beaded nanofiber surfaces. Permeability tests revealed that pure water permeability decreased markedly with decreasing CA content, whereas air permeability increased substantially with increasing CA content. These findings demonstrate that the synergistic interaction between PA6 and CA plays a critical role in determining both the structural integrity and filtration performance of composite membranes, and that PA6/CA composite nanofiber membranes produced by electrospinning have good potential for efficient, cost-effective, and scalable filtration material applications.

Keywords: membrane, filtration, electrospinning, nanofiber, Polyamide-6, cellulose acetate

INTRODUCTION

Water resources are becoming increasingly scarce due to the daily generation of tons of wastewater driven by rapid population growth.[1] Currently, many highly industrialized countries discharge 55% of their sewage without any treatment.[2] Furthermore, in low-income countries, more than 80% of discharged municipal wastewater remains untreated.[3] Consequently, this untreated wastewater leads to various environmental and human health issues. Considering the inefficiency, operational difficulties, high energy requirements, low economic benefits, and problems related to recyclability attributed to conventional treatment technologies, research has been driven towards innovative developments in technologies for the treatment of wastewater.[4]

In recent years, electrospun nanofibrous materials have garnered significant attention due to their exceptional characteristics, including high surface-to-volume ratios, nanoporosity, tunable surface chemistry, and robust mechanical strength. Their versatility in applications ranging from filtration and composites to biomedical fields has established them as critical components in both academic research and industrial sectors.[5] Electrospinning is widely recognized as a versatile method for fabricating fibers with diameters spanning the micro- to sub-micrometer scale.[6] In 1934, Formhals secured the initial patent for the electrospinning technique, a process that employs electrostatic forces to fabricate polymeric fibers.[7] In contrast to conventional fiber production techniques, such as melt, wet, and dry spinning, which rely on mechanical forces, electrospinning

employs electrostatic fields to elongate and stretch the polymer jet.[8,9] Upon the application of an electric field, the polymer solution acquires a charge and is ejected from the spinneret. As the resulting fine jet travels towards the collector, it experiences significant elongation and whipping instabilities. Concurrently, the rapid evaporation of the solvent leads to the solidification of the jet, which is then deposited as nanofibers.[10]

As illustrated in Figure 1, an electrospinning system with a rotating drum collector is composed of three primary elements: a fluid feeding mechanism, a high-voltage power source, and a rotating cylindrical collector.

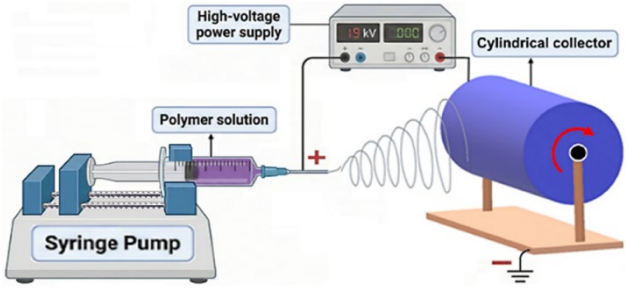


Figure 1: Basic components of an electrospinning system with cylindrical (rotating drum) collector

The variables influencing the electrospinning process are generally categorized into three distinct groups: parameters related to the polymer solution (molecular weight and viscosity, surface tension, solution conductivity and dielectric effect of the solvent),[11-13] parameters related to process conditions (voltage, solution feed rate (flow rate), collector type, distance between collector and needle tip, and needle diameter),[14,15] environmental parameters (temperature, relative humidity and pressure).[16] The nanofiber structure and morphology are governed by the complex interplay of these variables. For instance, while smaller needle diameters yield finer fibers, an increase in flow rate typically results in thicker fibers. Furthermore, although high voltage promotes fiber thinning, it may simultaneously result in the formation of beaded structures.[17]

As a highly versatile approach, electrospinning allows for the production of nanofibers utilizing various polymer-based solutions. The technique's rapid expansion, evidenced by a marked increase in literature since the 1990s, correlates directly with the global rise of nanotechnology. The fibers produced via this method – spanning from sub-micron to micrometer ranges – are characterized by their high specific surface area, flexibility, and superior mechanical performance. Consequently, electrospun materials have found widespread utility across multiple disciplines, including the fabrication of scaffolds for tissue engineering, wound healing systems, electronic devices, and environmental remediation technologies.[18] Key parameters affecting fiber fabrication via electrospinning include the polymer concentration, viscosity, conductivity, and the nature of the solvent. Solution concentration is particularly significant for maintaining the integrity of the nanofiber structure, largely because it correlates with viscosity and surface tension. Simultaneously, the solvent type plays a determining role by modifying the solution's surface tension and controlling the evaporation kinetics during the spinning process. Consequently, solvents possessing high volatility are known to alter the surface topography of the fibers and promote the formation of porous, web-like structures.[19] Electrospun polyamide fibers are well-established in various fields owing to the polymer's superior processability.[20-22]

PA stands out as a biodegradable, biocompatible material with enhanced mechanical properties due to hydrogen bonding, and unlike polyethylene oxide (PEO), it remains stable in humid environments. Furthermore, PA processing aligns with environmental safety standards by using formic or acetic acid rather than toxic solvents, such as DMF. Despite the popularity of PA6 and PA6.6 in research, their application to filtration has received limited attention.[23] Recent reports, however, indicate that PA is an exceptionally suitable material for developing high-performance filters.[21]

PA6 is a synthetic polymer distinguished by its favorable biocompatibility, biodegradability, and superior mechanical integrity. Typically, this material is synthesized via the ring-opening polymerization of the monomer ε-caprolactam.[24]

While PA6 holds a prominent position in the textile sector due to its versatility, it is also increasingly vital in biomedical research. In particular, the electrospinning technique is the preferred method for fabricating PA6-based nanofibrous scaffolds, as it yields constructs with the high robustness and biocompatibility required for tissue engineering.

Cellulose acetate (CA) is the most important ester of cellulose due to its low cost, non-toxicity, biodegradability, and renewable source.[25,26] Historically, CA has served as a foundational polymer in the fabrication of filtration membranes, being extensively engineered into modules for ultrafiltration, nanofiltration, and reverse osmosis. Its utility is well-established across critical sectors, including biotechnology, pharmaceuticals, and the food industry.[27] In recent years, the research focus has broadened beyond traditional separation processes to encompass emerging fields, such as membrane distillation, hydrophobic permeation, and unidirectional moisture transport. Owing to its excellent film-forming capabilities and renewable biomass origin, CA remains a preferred candidate for these novel membrane applications. However, it is crucial to acknowledge that the intrinsic hydrophilicity of CA is a limiting factor, restricting its direct application in processes that require hydrophobic interfaces, such as membrane distillation.[28]

In response to the shrinking availability of clean water resources and environmental pollution, the development of next-generation filtration technologies based on advanced nanomaterials has accelerated. Nanofibers represent a cutting-edge class of membranes characterized by extraordinary filtration capabilities. Their high porosity, which can be adjusted via manufacturing parameters, makes them highly effective for size-dependent separation. Therefore, it is imperative to conduct a thorough assessment of current nanofiber fabrication methods, analyzing their benefits and drawbacks. Furthermore, this paper explores the use of these membranes in the water treatment and desalination sectors to provide insights into emerging trends in membrane research.[29]

In filtration technologies, the membrane is the pivotal component, serving as a semi-permeable interface that separates two distinct phases. Generally, membrane-based processes are categorized by the specific driving mechanism (*e.g.*, pressure) and the barrier's pore size.[30] Figure 2 depicts the correlation between the specific pore diameters of membranes and the corresponding operational functions of various filtration systems.[31]

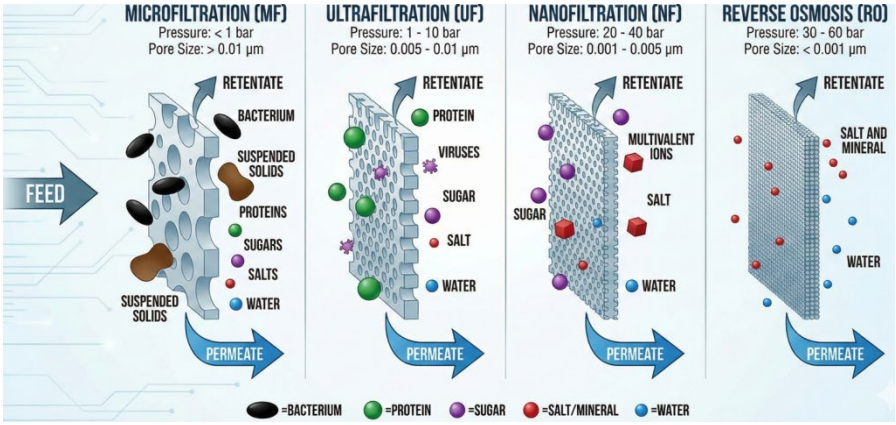


Figure 2: Classification of membranes based on their pore size and their retentate[5]

Due to its economic viability and robust mechanical profile characterized by high impact and tensile strength, PA6 serves as an ideal raw material. It also exhibits significant resistance to biological degradation by fungi and bacteria.[32-34] Conversely, CA is utilized for its antifouling properties, which are attributed to its hydrophilicity. Scientific literature suggests that fouling is largely induced by the hydrophobic interactions between membrane surfaces and biomolecules, which create high interfacial energy in aqueous environments.[35-37] CA overcomes this limitation by reducing protein adsorption through enhanced hydrophilicity. Coupled with properties, such as moderate flux, ease of fabrication, and renewability of its raw material, CA stands out as a highly effective polymer for the development of ultrafiltration membranes.[37]

This study presents an investigation into the interactions between (PA6) and (CA), specifically examining the dual effects of blend ratios and total solid content concentrations. The experimental framework involves a detailed analysis of both the polymer solution properties and the morphological characteristics of the resultant nanofiber membranes across various PA6/CA combinations. Consequently, the research focused on optimizing the fabrication process by systematically determining the ideal PA6/CA weight ratio and the optimal total solids percentage required to produce uniform nanofibrous membrane surfaces.

EXPERIMENTAL

Materials

Polyamide 6 (pellets, density: 1.084 g/mL at 25 °C (lit.), product number: 181110-500G); cellulose acetate (density: 1.3 g/mL at 25 °C (lit.) average Mn ~30,000 g/mol by GPC, 39.8 wt% acetyl, product number:180955-500G); acetic acid (CH_3COOH, 100%, density 1.049 g/mL at 25 °C (lit.)) product number: 27225-2.5L-R) and formic acid (HCOOH, >98%, density 1.22 g/mL at 25 °C (lit.) product number: 1.00264.2500) were purchased from Sigma Aldrich.

Preparation of polymer blend solutions

For the production of nanofiber membranes, PA6 and CA polymers were mixed in five different ratios (100/0, 75/25, 50/50, 25/75, and 0/100 by weight, respectively), and PA6/CA polymer solutions with a total solid content of 12% by weight were prepared. A binary solvent mixture of formic acid and acetic acid at a 1:1 weight ratio was used as the solvent system for preparing polymer solutions.

In the solution preparation process, formic acid and acetic acid were first mixed in a beaker with a magnetic stirrer set to heat for 10 minutes to obtain binary solvent mixtures. Then, CA was added to the binary solvent mixture. After approximately 30 minutes, PA6 was added, and the mixture was stirred at 600 rpm for 12 hours to obtain homogeneous solutions. Finally, the solution was processed in an ultrasonic bath at 30 °C for 30 minutes.

Membrane preparation

Electrospun nanofibers were produced by using the Inovenso brand NE300 model electrospining device, with a cylindrical collector (Fig. 3), in the Materials Research Laboratory of KSU ÜSKIM.

The prepared polymer solutions were drawn into a syringe, which was then placed into the electrospinning device. Subsequently, electrospinning parameters, such as power, feed rate, and nozzle-collector distance, during nanofiber spinning from polymer solutions were precisely set. The electrospinning process parameters used in this study to produce nanofiber membranes are listed in Table 1. Nanofibers were spun onto a 22*34 cm PP (polypropylene) spunbond fabric, which was wrapped around the cylindrical collector of the electrospinning device. The spunbond fabric remained as a permanent sub-layer within the membrane and served as a support layer. Some physical properties (*e.g.*, thickness, basis weight, porosity, and fiber diameter) of the polypropylene spunbond fabric are presented in Table 2.

Solution characterization

For the characterization of the polymer solutions used in membrane production, a PCE-RVI 2 viscometer was used for viscosity measurements, and a WTW PH7110 instrument was used for pH analyses.

Membrane characterizations

Structural characterization of membranes

The structural properties of nanofiber filter membranes produced by the electrospinning method were investigated by Fourier transform infrared spectroscopy with attenuated total reflectance (FTIR-ATR), using a Perkin Elmer Spectrum 400 instrument.

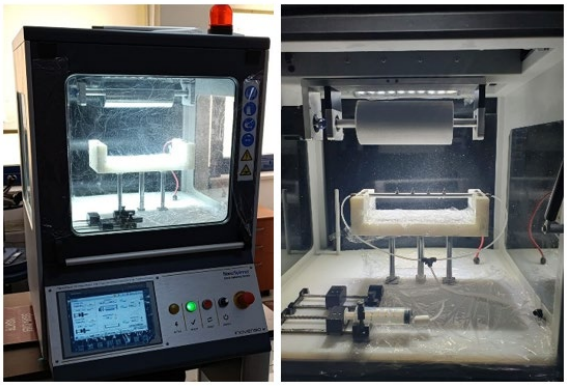


Figure 3: Inovenso NE300 model electrospinning device with a cylindrical collector

Table 1
Electrospinning process parameters

Sample code	PA6/CA ratio (%)	Total solid concentration (%)	Voltage (kV)	Distance (mm)	Feeding rate (mL/h)	Cylindrical collector		
						Rotational speed (rpm)	Stroke distance (mm)	Stroke speed (mm/s)
P100	100/0	12	25 - 30	100	1.5 - 3	100	80	20
P75	75/25							
P50	50/50							
P25	25/75							
P0	0/100							

Table 2
Average values of some physical properties of polypropylene spunbond fabric

Thickness (mm)	Basis weight (g/m^2)	Porosity (%)	Pore size (nm)	Fiber diameter (μm)
0.28	54.85	14.41	2246.57	26.64

Morphological characterization of membranes

The morphology of the nanofiber membranes was examined at the ÜSKİM laboratories of Kahramanmaraş Sütçü İmam University, using a ZEISS EVO LS10 Scanning Electron Microscope. All membrane samples were coated with a conductive layer of gold using a Cressington 108Auto gold plating device before SEM analysis to obtain high-resolution images. SEM images of samples prepared from each nanofiber membrane were taken at different magnifications, and morphological analyses were performed on them.

Mechanical characterization of membranes

To determine the mechanical properties of the produced nanofiber surfaces, strength tests were performed using a Zwick Roell Z5.0 tensile testing instrument.

Air permeability of membranes

Air permeability measurements of the produced samples were made in the Paper Research Laboratory of the Faculty of Forestry at Kahramanmaraş Sütçü İmam University, using a Gurley air permeability measuring device.

Pure water permeability of membranes

Performance tests of the membranes obtained by electrospinning were conducted against pure water. The tests were carried out using a vacuum membrane filtration system, in accordance with standard method TS 6465.

To determine the pure water permeability of the produced membranes, they were first soaked in pure water at room temperature for 120 minutes. The purpose of the soaking process is to prepare the membrane nanofibers for processing before the membrane flux treatment.

The flux of the produced membranes after wetting at a pressure of 0.6 bar was calculated according to Equation (1):

$$J_w = V/(A \times T) \quad (1)$$

where J_w is the flux ($L/m^2.h$), V is the filtrate volume (L), A is the membrane active area (m^2), and T is the time (hours). Permeability values were determined using the calculated flux value. Each sample was processed 10 times, and the average values were reported.[38-40]

The permeability value ($L/m^2.h.bar$) was obtained using Equation (2):[40]

$$Permeability = J_w/P \quad (2)$$

Porosity and pore size of membranes

To determine the filtration properties of the membranes, the permeability to pure water, porosity, and pore sizes were measured.

The porosity was determined by the gravimetric method, defined as:[41,42]

$$\varepsilon(\%) = \frac{W_w - W_d}{AL\rho} \times 100 \quad (3)$$

where W_w is the weight of the wet membrane, W_d is the weight of the dry membrane, ρ is the water density (0.998 g/cm^3), A is the effective area of the membrane (m^2), and L is the membrane thickness (m).

The mean pore radius was determined by the filtration velocity method. According to Guerout–Elford–Ferry equation, r_m can be calculated by the relation:[39,41,42]

$$r_m = \sqrt{\frac{(2{,}9 - 1{,}75\varepsilon) \times 8\eta LQ}{\varepsilon A \Delta P}} \quad (4)$$

where h is water viscosity, L is membrane thickness, and ΔP is operation pressure.

RESULTS AND DISCUSSION

In this study, polymer solutions were first prepared at different PA6/CA polymer ratios (100/0, 75/25, 50/50, 25/75, and 0/100). Nanofiber

membranes were then produced from these polymer solutions using the electrospinning method at a solution concentration of 12%. The polymer solutions and the prepared nanofiber membranes were characterized using a number of analytical techniques.

Solution characterization

Characterization tests were first performed to determine the pH, density and viscosity of the prepared solutions. The results of the performed tests are listed in Table 3.

Table 3
Solution formulations, their denotation and determined properties

Sample code	Solution preparation parameters			Measured solution properties		
	PA6 (%)	CA (%)	FA:AA ratio	pH	Density (g/mL)	Viscosity (cP)
P100	100	0	1:1	0.70	1.1219	371
P75	75	25	1:1	0.75	1.1132	215
P50	50	50	1:1	0.81	1.1133	292
P25	25	75	1:1	0.71	1.1150	340
P0	0	100	1:1	0.85	1.1160	727

Membrane characterization studies

The chemical structures of nanofiber filter membranes were investigated by FTIR, and their morphology was examined by SEM. Also, thickness, strength, and permeability tests of the nanofiber membranes were performed.

Fourier transform infrared (FTIR) spectroscopy analysis

The molecular structures and functional group modifications of PA6/CA blends prepared at various weight ratios (100/0, 75/25, 50/50, 25/75, and 0/100) were investigated using FTIR spectroscopy in the range of 4000–400 cm^{-1}. The spectra of the neat components and their blends are presented in Figure 4. The characteristic bands and their variations as a function of the blend composition were assigned as indicated below.

The 3300 cm^{-1} peak corresponds to the N-H stretching vibration characteristic of the amide group in Polyamide 6 (PA6). In the P100 (Neat PA6) spectrum, this peak appears sharp and distinct. As the PA6 content decreases (green-blue-red), the intensity of this peak diminishes significantly. In the P0 (Neat CA) spectrum, this region is dominated by the broader, weaker vibrations of residual hydroxyl (-OH) groups inherent to the cellulose acetate structure. The peak at 3090 cm^{-1} corresponding to the Fermi resonance of the N-H stretching vibration is also specific to PA6, and exhibits a direct correlation with the increasing polyamide concentration in the matrix.

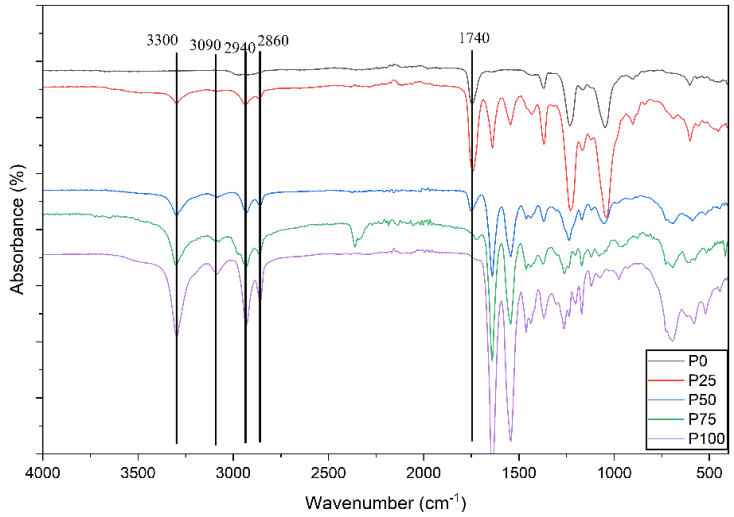


Figure 4: FTIR spectra obtained for formulations with different PA6/CA ratios

The bands at 2940 cm^{-1} and 2860 cm^{-1} are attributed to the asymmetric and symmetric C-H stretching vibrations of methylene (-CH_2-) and methyl (-CH_3) groups present in the backbones of both polymers. While observed in all spectra, the intensities of these peaks fluctuate with hydrogen density variations arising from changes in blend ratios.

The region 1750–1500 cm^{-1} provides the most critical spectral evidence for differentiating the components. At 1740 cm^{-1}, a sharp and intense peak represents the carbonyl (C=O) stretching vibration of the ester group in cellulose acetate (CA). It exhibits maximum intensity in the neat CA spectrum (P0). A systematic reduction in peak intensity is observed as the PA6 content increases (P25, P50, and P75). The complete absence of this peak in the neat PA6 spectrum (purple spectrum) confirms that it is a specific marker of CA content. Conversely, PA6-rich spectra show the emergence of Amide I (approx. 1640 cm^{-1}) and Amide II (approx. 1540 cm^{-1}) bands, which weaken as CA content increases.[43]

Scanning electron microscopy analysis

SEM images were obtained from each sample at magnification ratios of 1 kX, 5 kX, 10 kX, and 20 kX, and morphological examinations were performed on these images. SEM images at different magnifications of nanofiber surfaces produced by the electrospinning device from polymer solutions prepared by mixing PA6/CA at different ratios, as well as those of the spunbond fabric used as support are shown in Figures 5-10.

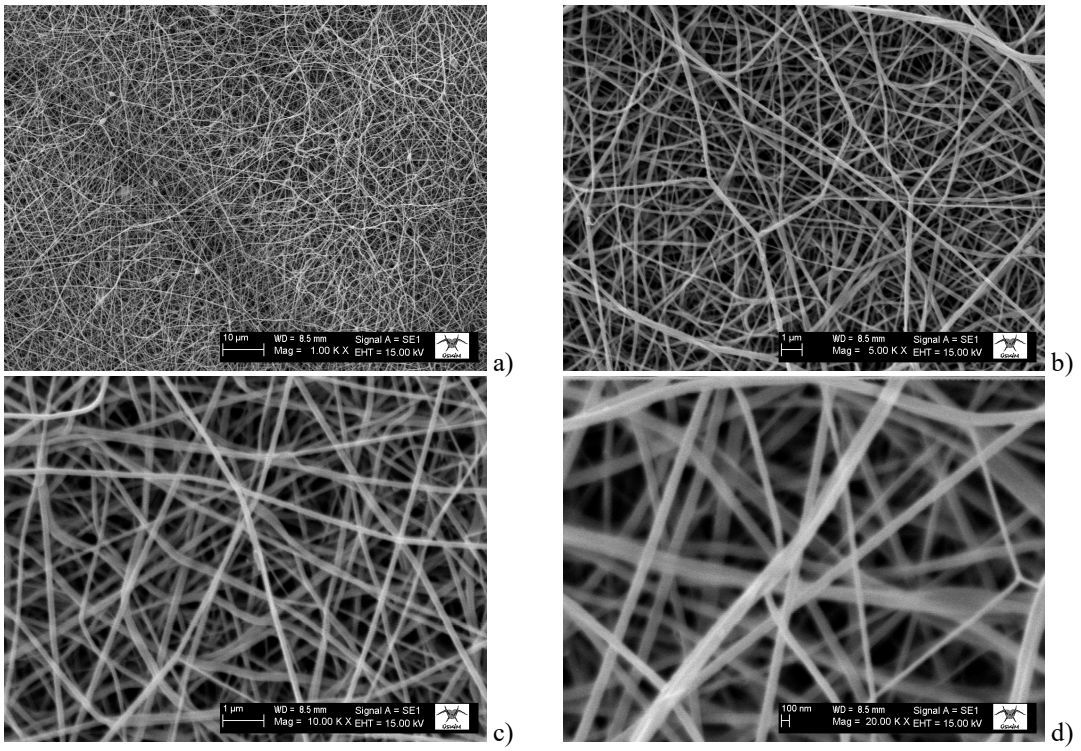
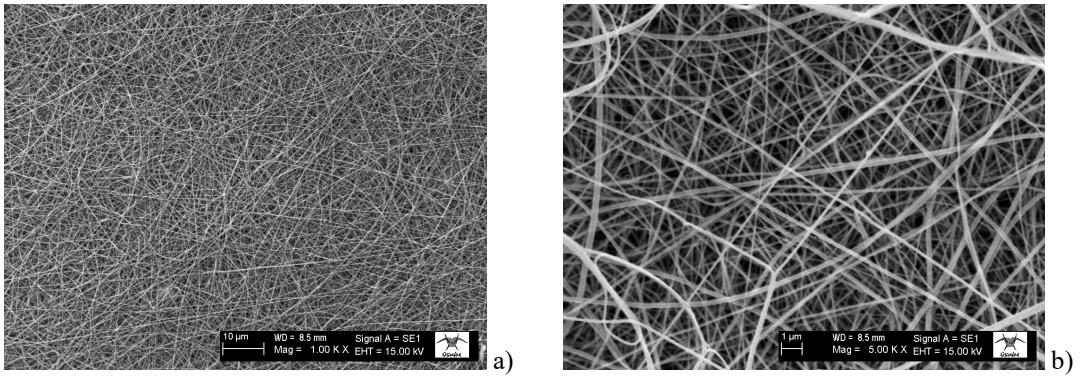
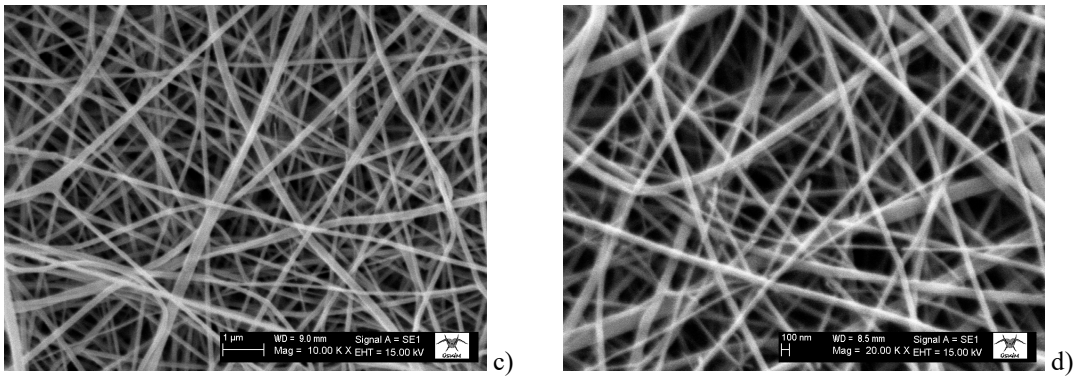


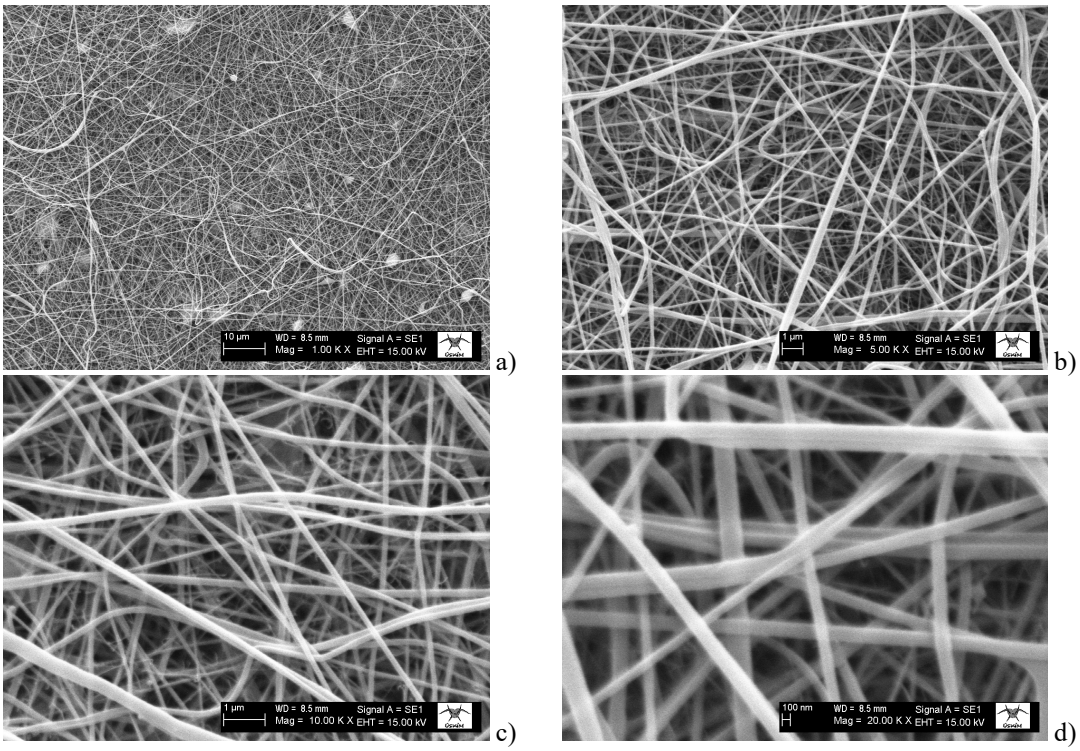
Figure 5: SEM images of P100 nanofiber surface samples at a) 1 kX, b) 5 kX, c) 10 kX and d) 20 kX





c) d)

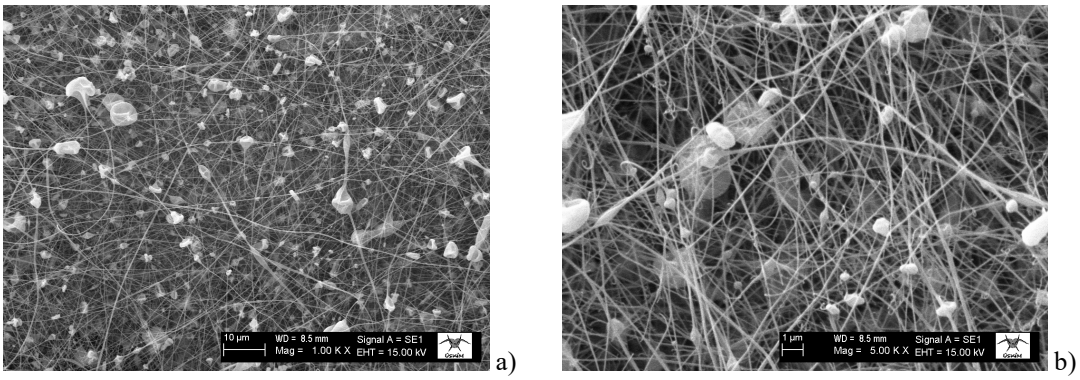
Figure 6: SEM images of P75 nanofiber surface samples at a) 1 kX, b) 5 kX, c) 10 kX and d) 20 kX



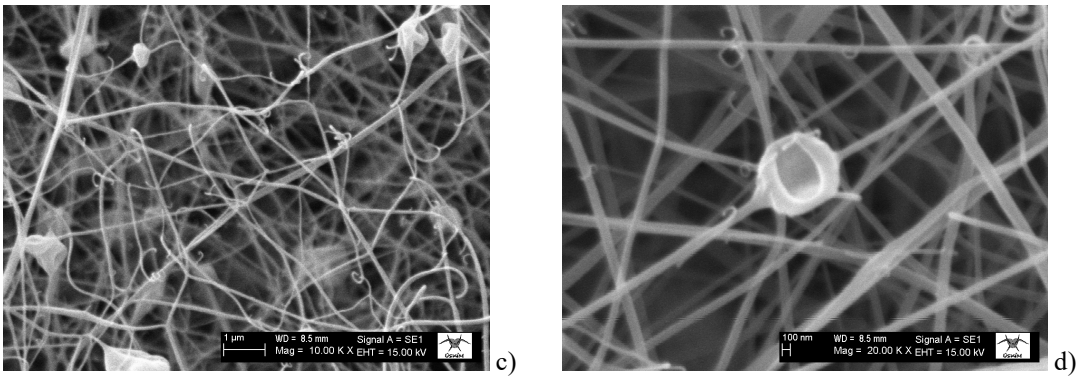
a) b)

c) d)

Figure 7: SEM images of P50 nanofiber surface samples at a) 1 kX, b) 5 kX, c) 10 kX and d) 20 kX

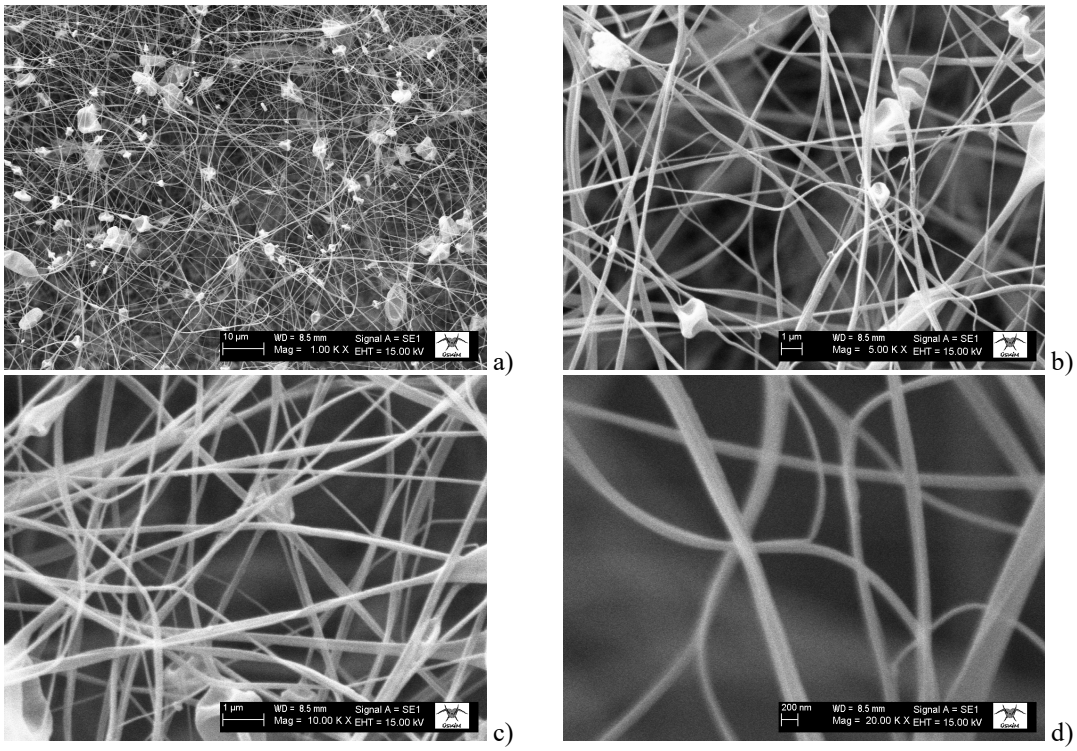


a) b)



c) d)

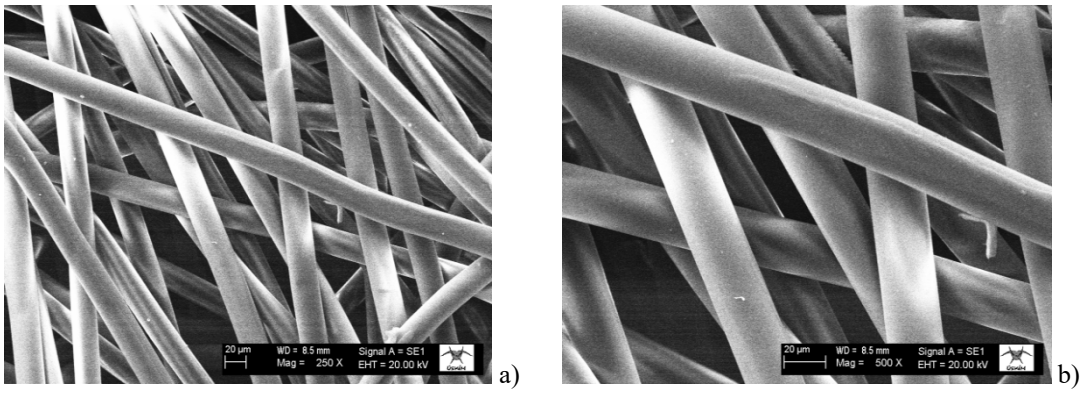
Figure 8: SEM images of P25 nanofiber surface samples at a) 1 kX, b) 5 kX, c) 10 kX and d) 20 kX



a) b)

c) d)

Figure 9: SEM images of P0 nanofiber surface samples at a) 1 kX, b) 5 kX, c) 10 kX and d) 20 kX



a) b)

Figure 10: SEM images of spunbond fabric sample at a) 250 X, b) 500 X

Table 4
Nanofiber fineness values on the produced nanofiber surfaces

Sample code	Nanofiber fineness (nm)	Standart deviation
P100	130	30.85
P75	115	38.08
P50	134	49.26
P25	145	56.62
P0	210	60.19

When the SEM images above are examined, the most uniform nanofiber structure is observed in samples obtained from PA6/CA polymer mixed at a ratio of 75/25. Furthermore, it was observed that a relatively more beaded structure was formed, especially when the CA ratio exceeded 50%. The nanofiber fineness values obtained from the SEM images are given in Table 4. Based on the fineness data from Table 4, it was observed that finer nanofiber structures were formed with decreasing CA content.

Membrane strength properties

The strength of the nanofiber membranes was determined in the production direction and the results are presented in Table 5. The graphs showing variation in strength and elongation of the membranes in the production direction are shown in Figures 11 and 12, respectively. As may be observed in Figures 11 and 12, when the CA content in the solution increases, both the strength and the elongation of the membranes in the production direction decrease.

The strength of the nanofiber membranes was also determined in cross-direction relative to the production direction of the collector, and the results are given in Table 6. The graphs showing the variation in strength and elongation values of nanofiber membranes in the vertical direction are given in Figures 13 and 14, respectively. When the results for the vertical direction are examined, it is observed that, as the CA content in the solution increases, both the strength and the elongation values of the nanofiber membranes decrease up to a certain point (sample P50), followed by an increase for higher proportion of CA.

Table 5
Strength results of nanofiber membranes obtained in the production direction

Sample code	Force (N)		Strain (%)	
	Mean	SD	Mean	SD
P100	13.16	0.28	15.8	0.18
P75	12.48	0.69	34.4	2.46
P50	12.34	0.50	22.0	2.01
P25	11.31	7.43	19.1	5.89
P0	8.66	4.28	21.8	9.23

Table 6
Strength results of nanofiber membranes determined in cross-direction

Sample code	Force (N)		Strain (%)	
	Mean	SD	Mean	SD
P100	4.57	3.96	32.68	0.49
P75	6.30	0.42	32.24	0.29
P50	5.73	1.26	16.67	5.37
P25	8.08	1.42	23.30	6.03
P0	12.63	7.84	21.76	9.68

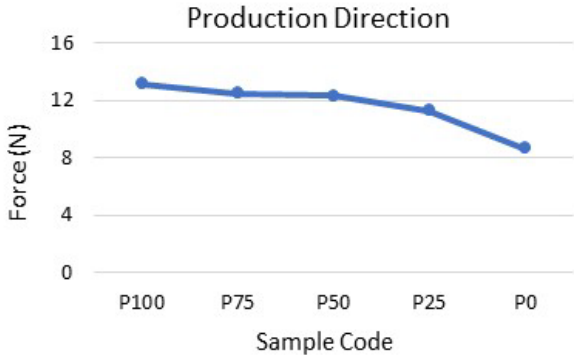


Figure 11: Variation of strength of nanofiber mats in the production direction (P)

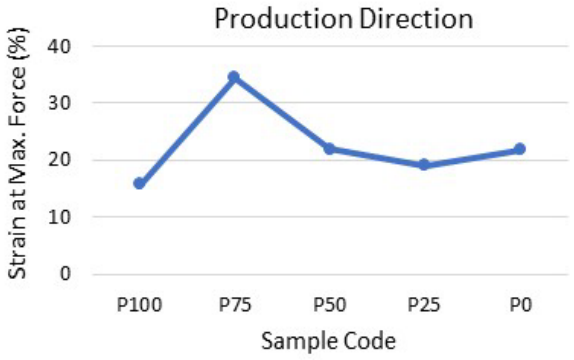


Figure 12: Variation of the strain at maximum force of nanofiber mats in the production direction (P)

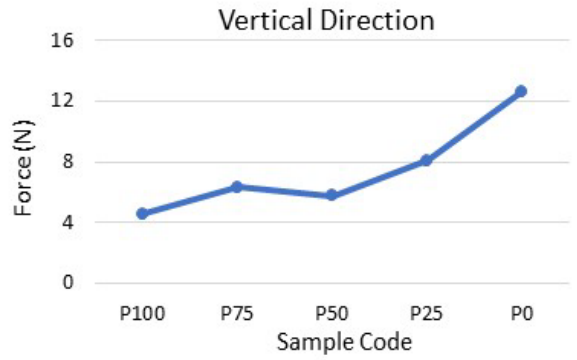


Figure 13: Variation of strength of nanofiber mats in cross-direction (V) relative to the collector

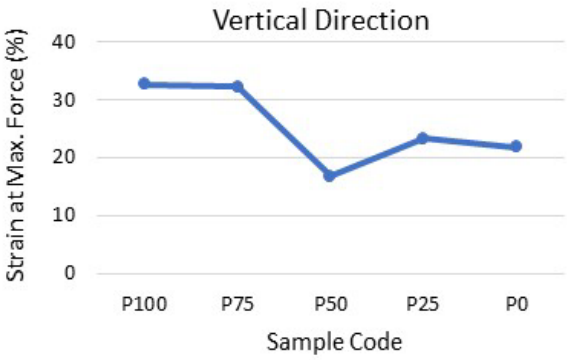


Figure 14: Variation of the strain at maximum force of nanofiber mats in cross-direction (V) relative to the collector

Air permeability

Air permeability measurements of the produced samples were carried out using a Gurley air permeability measuring device at the Paper Research Laboratory of the Faculty of Forestry at Kahramanmaraş Sütçü İmam University. With this device, air permeability is measured as the passage time (in seconds) of 100 cm³ of air through the sample. The values obtained are given in Table 7. Examining the air permeability values presented in Table 7 and Figure 15, it may be observed that, as the CA ratio increased, the air passage times of the samples decreased, consequently their air permeability values increased.

Pure water permeability

To assess the performance of the membranes produced, their pure water permeability was also assessed using a vacuum membrane filtration system, in accordance with TS 6465. The measured pure water permeability and flux values are given in Table 8.

Table 7
Air permeability values of the produced nanofiber surfaces

Sample code	Mean air permeability (s)
P100	13.14
P75	7.02
P50	4.38
P25	1.50
P0	1

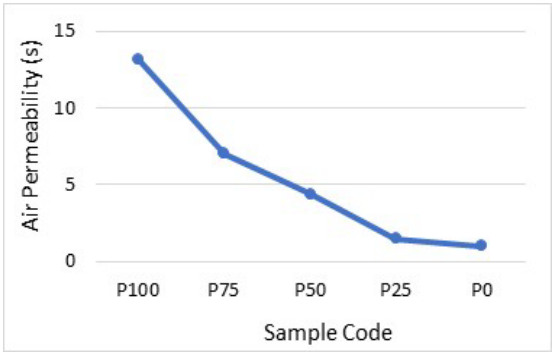


Figure 15: Variation of air permeability values of the produced nanofiber mats as a function of the PA6/CA mixing ratios

Table 8
Pure water permeability and flux values of PA6/CA membranes

Sample code	Flux, J_w (L/(m^2.h))	Permeability (L/(m^2.h.bar))
P100	6340.43	10567.39
P75	9434.06	15723.44
P50	12388.37	20647.28
P25	160562.44	267604.07
P0	101080.26	168467.10

It is known that various factors – such as surface pore size, cross-sectional morphology, membrane thickness, and hydrophilicity – collectively determine the membrane's permeation and flux. Additionally, the PA6/CA blend ratio influences the permeability and flux of pure water. As shown in Figures 16 and 17, the pure water permeability and flux of the nanofiber mats increased with rising CA content in the formulation, peaked at the formulation P25, and subsequently decreased slightly. When data from Tables 4 and 8 are evaluated together, it is evident that permeability and flux values increase as the fiber diameter increases. Similarly, an evaluation of Tables 8 and 9 reveals that permeability and flux values rise with increasing porosity and pore size. The pore size value also peaks in sample P25, indicating that pore size has a more significant impact on permeability and flux values.

Porosity and pore size

The measured porosity and pore size values are given in Table 9. It is observed that the fiber diameter increases with an increase in the CA content of the polymer blend (Table 4), and that porosity and average pore diameter increase as the fiber diameter increases (Table 9). Thus, the proportion of cellulose acetate (CA) in the polymer solution had an influence on the porosity and pore size values of the produced nanofiber mats.

Table 9
Porosity and pore size values of PA6/CA membranes

Sample code	Porosity, ε (%)	Average pore size, r_m (μm)
P100	84.81	0.2910
P75	85.94	0.3246
P50	78.49	0.4120
P25	88.65	0.9265
P0	98.94	0.9180

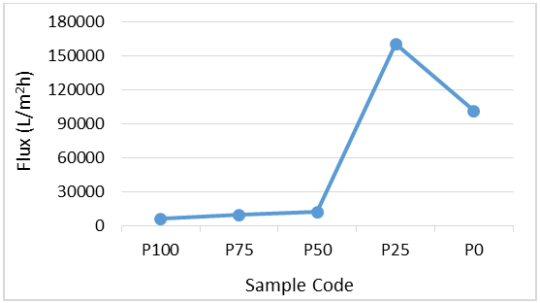


Figure 16: Variation of flux values of produced nanofiber mats as a function of PA6/CA mixing ratios

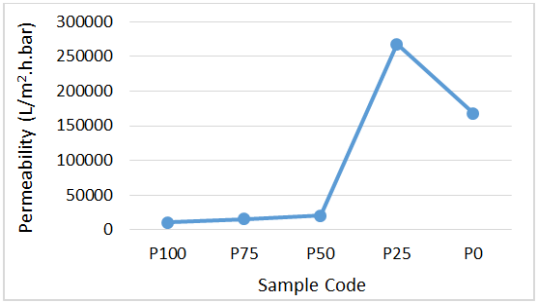


Figure 17: Variation of pure water permeability values of produced nanofiber mats as a function of PA6/CA mixing ratios

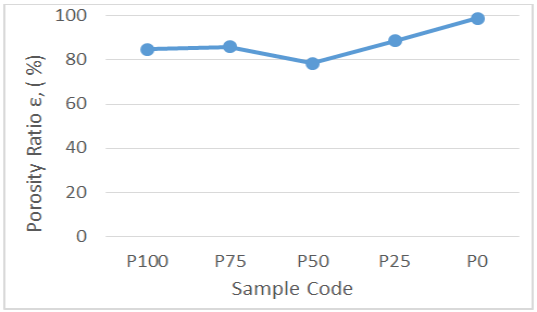


Figure 18: Variation of porosity ratio values of produced nanofiber mats as a function of PA6/CA mixing ratios

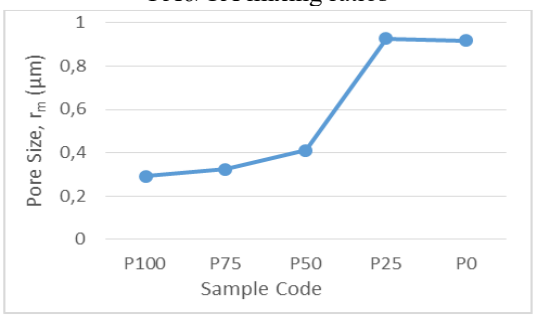


Figure 19: Variation of pore size values of produced nanofiber mats as a function of PA6/CA mixing ratios

Correlation analysis was performed in SPSS to assess the relationship between membrane permeability and other membrane properties. Since the data were not normally distributed, Spearman's Rho correlation analysis, which is a non-parametric correlation analysis, was preferred. The results of the correlation analysis are given in Table 10.

Considering the data listed in Table 10, it can be determined that the correlation coefficient between pure water permeability and flux and pore size is 1.000; therefore, there is a very strong relationship among them; these correlations are statistically significant at the 0.01 level. These results indicate that pure water permeability correlates most strongly with flux and pore size, and therefore, these properties are the most important characteristics affecting pure water permeability, which supports the rising values of pure water permeability with increasing flux and pore size.

The correlation coefficient between pure water permeability and air permeability is -0.900, indicating a strong negative correlation. Since the air permeability measurement is based on the passage time of 100 cm^3 of air through the membrane, the air permeability of the produced membrane increases as the air passage time decreases. Therefore, as the air passage time decreases (*i.e.*, as air permeability increases), the pure water permeability value also increases.

Table 10
Correlation analysis results

Correlations (Spearman's Rho)							
Parameter		Pure water permeability	Flux	Air permeability	Pore size	Porosity	Fiber diameter
Pure water permeability	Correlation coefficient (ρ)	1	1.000**	-0.900*	1.000**	0.600	0.800
	Sig. (2-tailed)	-	0.000	0.037	0.000	0.285	0.104
Air permeability	Correlation coefficient (ρ)	-0.900*	-0.900*	1	-0.900*	-0.700	-0.900*
	Sig. (2-tailed)	0.037	0.037	-	0.037	0.188	0.037

*Correlation is significant at the 0.05 level (2-tailed); **Correlation is significant at the 0.01 level (2-tailed)

The correlation coefficient between pure water permeability and fiber diameter was 0.800. Although this coefficient indicates a strong relationship between the two properties, the relationship was not statistically significant at the 0.05 level (α=0.104). Nevertheless, this means that fiber diameter affects permeability.

The correlation coefficient between pure water permeability and porosity was 0.600. Although this coefficient indicates a moderate relationship between the two properties, the relationship was not statistically significant at the 0.05 level (α=0.285). This means that porosity values have less effect on pure water permeability.

As stated above, because the air permeability values were measured by passing 100 cm^3 of air through the membrane, the correlation coefficients between air permeability and the other characteristics examined in this study were negative. However, because a decrease in passage time indicates increased air permeability, these were evaluated positively. It was determined that the correlation coefficients between air permeability and flux, pore size, and fiber diameter were -0.900; therefore, there was a very strong relationship, and these correlations were statistically significant at the 0.05 level (observed). These results indicate that air permeability correlates most strongly with flux, pore size, and fiber diameter, and therefore, these are the most important membrane characteristics affecting air permeability. Consequently, air permeability increases with increasing flux, pore size, and fiber diameter. The correlation coefficient between air permeability and porosity was -0.700. Although this coefficient indicates a strong relationship between the two properties, the relationship was not statistically significant at the 0.05 level (α=0.188). Nevertheless, this means that porosity values affect pure water permeability.

Reports in the literature have often deminstrated the relation between average pore size and average fiber diameter in nanofibers.[44,45] This study also found that one of the most important parameters affecting the permeability of pure water and air is pore size. Naturally, a larger pore diameter will result in larger diffusion channels for air and water permeability.

CONCLUSION

In this study, novel composite nanofiber membranes based on PA6 and CA blends were successfully developed via electrospinning for high-performance filtration applications. An investigation into the effects of the blend ratio (100/0, 75/25, 50/50, 25/75, and 0/100) on solution properties, fiber morphology, and filtration performance yielded the following key conclusions:

1) The characteristics of the spinning solutions were governed by the blend composition. Increasing the PA6 content resulted in a systematic decrease in solution viscosity and an increase in pH, attributed to the flexible chain nature and proton-accepting amide groups of PA6, respectively.

2) SEM analysis confirmed that defect-free and uniform nanofibers were produced across all blend ratios. Notably, a direct correlation was observed between polymer composition and fiber diameter; the finest fiber diameter (approx. 115 nm) was achieved with the PA6-rich (75/25) blend, indicating that PA6 facilitates the formation of finer network structures.

3) FTIR spectra validated the physical blending of the polymers, without chemical cross-linking, where the intensity of the characteristic ester carbonyl peak at 1740 cm^{-1} served as a precise marker for CA content.

4) The study revealed a critical trade-off between mechanical integrity and permeability. While PA6 contributed to the mechanical robustness of the membranes (higher tensile strength), incorporating CA significantly enhanced hydrophilicity and flux. Specifically, the CA-rich membranes exhibited superior permeability to pure water and air, making them highly efficient for high-flux filtration.

5) It has been found that pore size is the most significant parameter affecting membrane permeability characteristics, while fiber diameter also has a notable influence.

To conclude, this research demonstrates that PA6/CA electrospun membranes offer a tunable platform where the filtration efficiency and mechanical stability can be optimized by adjusting the blend ratio. The synergistic combination of PA6's mechanical strength and CA's excellent flux properties positions these composite membranes as promising and cost-effective candidates for next-generation water treatment technologies.

ACKNOWLEDGEMENT: This study was supported by the Scientific and Technological Research Council of Turkey (TÜBİTAK) under project number 123Y461 and by the

Kahramanmaraş Sütçü İmam University (KSÜ) Research and Development Unit under project number 2024/8-10 D. We would like to thank TÜBİTAK and the KSÜ Research and Development Unit for their support of this study. A portion of this study was presented as an abstract at the IV International Korkut Ata Scientific Research Congress.

REFERENCES

[1] T. U. Rashid, S. F. Kabir, M. C. Biswas and M. R. Bhuiyan, *Ind. Eng. Chem. Res.*, **59**, 9719 (2020), https://doi.org/10.1021/acs.iecr.0c00676

[2] M. A. I. Islam, M. F. Rahman, M. M. İslam, M. K. Mohammed and A. İrfan, *Phys. Chem. Chem. Phys.*, **27**, 1861 (2025), https://doi.org/10.1039/D4CP04276J

[3] M. N. Hossain, M. D. Islam, A. Rahaman, N. Khatun and M. A. Matin, *Appl. Water Sci.*, **13**, 1 (2023), https://doi.org/10.1007/s13201-023-01879-5

[4] M. D. Islam and M. M. Mahdi, in "Biodegradation and Detoxification of Micropollutants in Industrial Wastewater", edited by I. Haq, A. S. Kalamdhad and M. P. Shah, Elsevier, 2022, pp. 1–26, https://doi.org/10.1016/B978-0-323-88507-2.00011-7

[5] W. E. Teo and S. Ramakrishna, *Nanotechnology*, **17**, R89 (2006), https://doi.org/10.1088/0957-4484/17/14/R01

[6] A. Kılıç, F. Oruc and A. Demir, *Text. Res. J.*, **78**, 532 (2008), https://doi.org/10.1177/0040517507081296

[7] F. Anton, U.S. Patent 1,975,504. Washington DC: U.S. Patent and Trademark Office, 1934

[8] P. Danwanichakul, D. Danwanichakul, N. Sueviriyapan and B. Sumruan, in *Procs. The 1st Mae Fah Luang University International Conference*, Pathumthani, Thailand, 2012, pp. 1–8

[9] G. S. Kozanoğlu, MSc. Thesis, İstanbul Thecnical University, İstanbul, Türkiye, 2006

[10] İ. Tiyek, A. Gündüz, F. Yalçınkaya and J. Chaloupek, *J. Nanosci. Nanotechnol.*, **19**, 7251 (2019), https://doi.org/10.1166/jnn.2019.16605

[11] S. Ramakrishna, K. Fujihara, W. E. Teo, T. C. Lim, Z. Ma, "An Introduction to Electrospinning and Nanofibers", World Scientific Publishing, Singapore, 2005, p. 3-86

[12] R. Rangkupan, PhD Thesis, University of Akron, 2002

[13] K. Paipitak, T. Pornprac, P. Mongkontalang, W. Techitdheera and W. Pecharapa, *Proc. Eng.*, **8**, 101 (2011), https://doi.org/10.1016/j.proeng.2011.03.019

[14] T. J. Sill and H. A. Recum, *Biomaterials*, **29**, 1989 (2008), https://doi.org/10.1016/j.biomaterials.2008.01.011

[15] X. Zong, K. Kim, D. Fang, S. Ran, B. S. Hsiao, B. Chu, *Polymer*, **43**, 4403 (2002), https://doi.org/10.1016/S0032-3861(02)00275-6

[16] N. Bhardwaj and S. C. Kundu, *Biotechnol. Adv.*, **28**, 325 (2010), https://doi.org/10.1016/j.biotechadv.2010.01.004

[17] J. M. Deitzel, J. Kleinmeyer, D. E. A. Harris and N. C. Beck Tan, *Polymer*, **42**, 261 (2001), https://doi.org/10.1016/S0032-3861(00)00250-0

[18] J. Kerwald, C. F. de Moura Junior, E. D. Freitas, J. D. P. de Moraes Segundo, R. S. Vieira *et al.*, *Cellulose*, **29**, 25 (2022), https://doi.org/10.1007/s10570-021-04303-w

[19] R. Nirmala, K.T. Nam, S. J. Park, Y. S. Shin, R. Navamathavan *et al.*, *Appl. Surf. Sci.*, **256**, 6318 (2010), https://doi.org/10.1016/j.apsusc.2010.04.010

[20] M. Chowdhury and G. Stylios, *Int. J. Basic Appl. Sci.*, **10**, 70 (2010)

[21] H. R. Pant, M. P. Bajgai, C. Yi, R. Nirmala, K. T. Nam *et al.*, *Colloids Surf. A*, **370**, 87 (2010), https://doi.org/10.1016/j.colsurfa.2010.08.051

[22] B. De Schoenmaker, L. Van der Schueren, Ö. Ceylan and K. De Clerck, *J. Nanomater.*, **2012**, 860654 (2012), https://doi.org/10.1155/2012/860654

[23] C. H. Hung and W. W. F. Leung, *Sep. Purif. Technol.*, **79**, 34 (2011), https://doi.org/10.1016/j.seppur.2011.03.008

[24] Wikipedia, Nylon 6, https://en.wikipedia.org/wiki/Nylon_6

[25] I. O. Fortu, C. Negoescu and I. Mamaliga, *Cellulose Chem. Technol.*, **53**, 527 (2019), https://doi.org/10.35812/CelluloseChemTechnol.2019.53.53

[26] F. E. Tabaght, A. El Idrissi, M. Aqil, A. Benahemad, S. El Barkany *et al.*, *Cellulose Chem. Technol.*, **54**, 207 (2020), https://doi.org/10.35812/CelluloseChemTechnol.2020.54.23

[27] Y. Tao, Y. Dai, Z. Zhang, M. Geng, F. Liu *et al.*, *Carbon*, **202**, 276 (2023), https://doi.org/10.1016/j.carbon.2022.10.087

[28] G. Tedeschi, S. Guzman-Puyol, U. C. Paul, M. J. Barthel, L. Goldoni *et al.*, *Chem. Eng. J.*, **348**, 840 (2018), https://doi.org/10.1016/j.cej.2018.05.031

[29] H. Saleem, L. Trabzon, A. Kılıç and S. J. Zaidi, *Desalination*, **478**, 114178 (2020), https://doi.org/10.1016/j.desal.2019.114178

[30] M. Aslan, "Membran teknolojileri", T.C. Çevre ve Şehircilik Bakanlığı, TUÇEV Türkiye Çevre Koruma Vakfı Yayınları, Ankara, Türkiye, 2016

[31] R. Abu-Zurayk, N. Alnairat, A. Khalaf, A. A. Ibrahim and G. Halaweh, *Processes*, **11**, 489 (2023), https://doi.org/10.3390/pr11020489

[32] L. Li, L. M. Bellan, H. G. Craighead and M. W. Frey, *Polymer*, **47**, 6208 (2006), https://doi.org/10.1016/j.polymer.2006.06.049

[33] Q. Li, Q. Wei, N. Wu, Y. Cai and W. Gao, *J. Appl. Polym. Sci.*, **107**, 3535 (2008), https://doi.org/10.1002/app.27529

[34] Y. Polat, M. Çalışır, M. Güngör, M. N. Sağırlı, R. Atakan *et al.*, *J. Ind. Text.*, **51**, 821 (2021), https://doi.org/10.1177/1528083719888674

[35] M. Sivakumar, D. R. Mohan and R. Rangarajan, *J. Memb. Sci.*, **268**, 208 (2006), https://doi.org/10.1016/j.memsci.2005.06.017

[36] A. Jayalakshmi, S. Rajesh and D. Mohan, *Appl. Surf. Sci.*, **258**, 9770 (2012), https://doi.org/10.1016/j.apsusc.2012.06.028
[37] Y. An, F. Li, Y. Di, X. Zhang, J. Lu *et al*., *Molecules*, **29**, 5127 (2024), https://doi.org/10.3390/molecules29215127
[38] H. Aburideh, Z. Tigrine, D. Zioui, S. Hout, D. Tsallait *et al*., *Cellulose Chem. Technol*., **55**, 697 (2021), https://doi.org/10.35812/CelluloseChemTechnol.2021.55.59
[39] C. Liao, J. Zhao, P. Yu, H. Tong and Y. Luo, *Desalination*, **285**, 117 (2012), https://doi.org/10.1016/j.desal.2011.09.042
[40] C. Liu and R. Bai, *J. Membr. Sci*., **267**, 68 (2005), https://doi.org/10.1016/j.memsci.2005.06.001
[41] M. Islam, J. McCutcheon and M. Rahaman, *J. Membr. Sci*., **537**, 297 (2017), https://doi.org/10.1016/j.memsci.2017.05.019
[42] J. F. Li, Z. L. Xua, H. Yanga, L. Y. Yua and M. Liu, *Appl. Surf. Sci*., **255**, 4725 (2009), https://doi.org/10.1016/j.apsusc.2008.07.139
[43] A. Gül and İ. Tiyek, *Int. J. Chem. Technol*., **7**, 91 (2023), https://doi.org/10.32571/ijct.1207544
[44] İ. Yağmur Mol, F. Cengız Çallıoğlu, H. Kesici Güler, E. Sesli Çetin and G. Bilir, *Cellulose Chem. Technol*., **57**, 79 (2023), https://doi.org/10.35812/CelluloseChemTechnol.2023.57.08
[45] J. McCann and D. Bryson, "Textile-Led Design for the Active Ageing Population", Elsevier, 2014, pp. 551